

The Technology of Nb Production and Purification

H. Padamsee
Lab of Nuclear Studies
Cornell University

This talk is divided into three parts. In the first I shall discuss what aspects of Nb metal RF cavity builders should be concerned with and the reasons for these concerns. The technology of Nb production and the procedures which have most bearing on achieving the desirable properties will be discussed in the second part. Here I shall try to delineate where possible improvements can be forthcoming. In the last part I shall discuss methods of improving Nb purity after production.

I. Nb Properties Specifications

The desirable properties of Nb we buy to make superconducting rf cavities can be specified in three categories

- a) Surface Texture
- b) Workability
- c) Purity

I omit some of the obvious, but important, dimensional tolerance specifications essential to manufacturability.

a. Surface Texture

The main reason to be concerned with surface texture is to avoid defects that can lead to thermal breakdown. I shall only briefly discuss this category as G. Muller will be discussing defect classification and diagnostic methods in detail in the next talk. We can specify that the Nb be free of embedded inclusions, deep scratches and surface cracks. We may further specify that the Nb sheet not be ground as is standard finishing practice in most industries, because grinding tends to camouflage residual surface cracks. Problems in this area can be readily determined by visual inspection, anodization followed by microscopic examination for discolorations, and soaking the Nb in water for some hours to look for iron inclusions that rust. A very useful tool in the inspection would be SLAM (scanning laser acoustic microscopy)⁽¹⁾ which can rapidly scan large areas, picking out cracks as well as interior and surface inclusions larger than 50 μm .

b. Workability

Spherical and elliptical Nb cavities are today made by spinning and deep drawing. Both operations require good cold working properties for sheet Nb. These are determined by small grain size and near 100% crystallized Nb. Figure 1 shows the scale of ASTM grain sizes 3 to 8. Good workability is achieved with the finer grains, 5 to 6 being the minimum desirable size, corresponding to 50 to 70 μm . Both grain size and recrystallization fraction are determined by straightforward metallographic techniques.

c. Purity

This issue has only come to the forefront in the last few years. Its major importance is due to the influence that the interstitial impurities, O, N, C and H have on the thermal conductivity of Nb. As shown in Figure 2, computer simulations of thermal breakdown in Nb cavities⁽²⁾ show that a given defect will breakdown at a higher field level if the thermal conductivity of the Nb is increased. The field level increases roughly as the $\sqrt{\text{RRR}}$, the residual resistivity ratio, which, as I shall discuss in more detail, is a convenient measure of the Nb thermal conductivity as well as the overall Nb purity. In Figure 2b we compare calculations of the thermal model with RF test results on 8 X-band elliptical Nb cavities with RRR values between 25 and 1400. In the calculations of Figure 2a we have used the detail temperature dependent thermal conductivities shown in Figure 3.

There are several methods to evaluate the purity of Nb. Primarily we are concerned with interstitially dissolved gases O, N, H as well as interstitial C. These have a far greater effect in lowering the electron mean free path than other impurities. A measurement of the residual electrical resistance at low temperatures provides a convenient guage of the total impurity content. It has become customary to quote this value in the form of a ratio = electrical resistance at room temperature (=14.5 $\mu\Omega\text{-cm}$)/electrical resistance at low temperature, typically 4.2 K⁺. In Table 1 I list the RRR values for 1 wt ppm of the most commonly found impurities.⁽³⁾

Since Nb is superconducting at 4.2 K it is necessary to drive it into the normal state with a d-c magnetic field higher than $H_{c3} = 1.7 H_{c2} \sim 4$ kGauss. Higher fields may be necessary if H_{c2} is locally enhanced due to work damage (dislocations).

Residual resistivity measurements have been performed at Cornell on various sheets of commercial grade Nb purchased from Wah Chang, KBI, Fansteel, and CBMM (Brazil).⁽⁴⁾ The sheet thicknesses range from .005" to 0.125". Results plotted in the histogram, Figure 4, show that most commercial Nb used in cavity production has an RRR between 20 - 30.

A second method to characterize Nb purity is to measure the thermal conductivity in the superconducting (SC) state. The theoretical calculations of Kadanoff & Martin⁽⁵⁾ give the ratio of the thermal conductivity in the SC state, K_S , to the thermal conductivity, K_N , in the normal state, and the Wiedemann Franz Law⁽⁶⁾, $K_N = L_0 T/\rho$, relates the normal thermal conductivity to the resistivity. From these, a convenient relationship

$$RRR = 400 K_S (4.2 \text{ k}) \text{ watts/m-k}$$

is derived.

While it is most convenient for SC cavity application to use one of the two methods so far discussed to determine the overall Nb purity, it is also important to know the individual impurity constituents to devise methods to produce purer Nb. I shall therefore make a short digression to discuss some of the direct methods for measuring gaseous impurities. In this discussion it is also appropriate to mention methods used to measure metallic impurities.

A brief overview of the various methods, their domain of applications and sensitivities is shown in Table 2.⁽⁷⁾ For metallic impurities the common methods are emission spectrography⁽⁸⁾ and spark source mass spectrometry,⁽⁹⁾ the second being more sensitive. The less common methods are activation analysis,⁽¹⁰⁾ using slow or fast neutrons, protons as well as γ radiation for activation. In emission spectrometry, a small portion of the sample is volatilized in a discharge and a fraction of the free atoms raised to an excited state. By analyzing the radiation from the discharge, the chemical composition is deduced from the location of the spectral lines. The line intensities, suitably calibrated, serve as a basis for quantitative analyses.

In spark source mass spectrometry, a spark is initiated between two electrodes made of the sample material. The positive ions produced are accelerated and analyzed in a double focussing mass spectrometer. This method has also been applied successfully to quantitative determination of O, N, C and H if the vacuum of the source and analyzer regions are maintained clean

and with low outgassing rates.⁽⁹⁾ A recently perfected refinement⁽¹¹⁾ uses a laser for a source and provides absolute concentrations without use of standards. This is possible from known ionization coefficients as a function of laser power density, and by controlling the power density.

The classical methods for O, N, C and H determination involve extraction of the impurities in the form of gases, followed by separation and quantitative measurement.⁽¹²⁾ In vacuum fusion extraction, used for O, N and H, a weighed metal sample is melted in vacuum inside a crucible sometimes in the presence of a flux such as Pt to keep the charge molten. The crucible may be graphite in which case O is removed as CO. In inert gas fusion a carrier gas, such as Ar, is used to sweep out the evolving gas. In hot vacuum extraction a solid sample is heated in a vacuum, UHV if necessary, and the gases evolve by diffusion. The released gases are measured by the increase of pressure using a thermal conductivity cell or other sensitive pressure gauge. In the case of CO, the gas is converted to CO₂ by passing over a hot CuO catalyst and the quantity of CO₂ measured by pressure change or by infra-red absorption or by changes in conductivity of a solution of BaOH (or NaOH).⁽¹³⁾ The C content of Nb can be similarly determined in a fusion apparatus using a flowing stream of O₂ to convert C into CO.

How close do the classical methods of measuring the interstitials come to agreement with RRR measurements?² Table 3 compares analyses provided by four companies with RRR measurements performed at Cornell. On the average a 20% discrepancy remains in the comparison.

To summarize the specifications section, from the many years of experience building and testing Nb cavities for accelerators the surface quality, workability and purity requirements can be accurately specified and measured.

II. Technology of Nb Production

I shall trace the various steps in the production of sheet Nb and point out some areas of necessary control and potential improvement in the various stages of manufacture. In this discussion, the various procedures for extracting Nb metal from the ore will be omitted, except for the remark that if in the future it becomes necessary to limit the Ta content, several suppliers have

shown it possible to keep the Ta content low by careful selection.

After extraction, electron beam melting is the main purification method. (14)
 In Figure 5 I show two typical setups for electron beam furnaces. The beam is arranged to hit both the feedstock as well as the top of the ingot to maintain a molten pool. As the tip of the ingot melts, molten metal globules fall into a pool on the ingot which is contained in a water cooled copper sleeve or cylinder. Impurities are boiled out of the pool and pumped away. Power impact is maintained to keep the pool molten out to within a few mm of the crucible wall. As melting progresses, the ingot formed is continuously withdrawn through the sleeve. The rate of withdrawal has to be carefully coordinated with the melt rate of the raw material to insure thorough melting of the feed material and proper outgassing of the formed ingot.

The outgassing of Nb at high temperatures is described by the following reaction and equilibrium equations (Table 4).¹⁵

Hydrogen desorbs readily from Nb at temperatures above 800°C; two dissolved H atoms combine to form molecular H₂ which then desorbs from the surface of the Nb. The removal of oxygen takes place by evaporation of NbO and NbO₂ from the metal surface. The removal of N from Nb is governed by the formation and evaporation of N₂. Carbon desorbs only as CO. For high O content Nb, both decarburization via CO as well as removal of O via NbO (NbO₂) takes place. For low O content, only a volatile oxide forms. Thus insufficient O can leave a few ppm of C in Nb which can only be removed by annealing in an O atmosphere (eg. 10⁻⁵ torr at 1650°C) to establish an excess O surface coverage.

From the average of several ingot analyses supplied by manufacturer's of commercial grade pure Nb, we found <O> = 100 ppm, <N> = 30 ppm, <C> = 30 ppm, implying <RRR> = 30. Using relations in Table 4 at the melting temperature of Nb (2450°C) we conclude that P_{O₂} = 10⁻⁴ torr, P_{N₂} = 4 x 10⁻⁵ torr and P_{CO} ~ 10⁻⁴ torr, resulting in a total pressure estimate ~ 2.5 x 10⁻⁴ torr, roughly consistent with pressure readings of industrial vacuum furnaces. (Note that if the O content is attributed to water vapor it would imply a partial pressure of 4 x 10⁻⁴ torr which seems improbably high unless a water leak were present.) If the partial pressures of O₂, N₂ and CO could be reduced to 1 x 10⁻⁵ torr each, then:

$$C_O = 9, C_N = 14.5, C_C = 2.44/C_O \\ \rightarrow RRR = 184 \text{ (neglecting C)}$$

Thus it would seem that major gains in purity should be possible by improving the quality of the vacuum in industrial e-beam furnaces.

As shown by the equations in Table 4, an alternative approach is to raise the temperature of the molten pool at the top of the ingot by applying more power. Table 5 shows that substantial gains in RRR can be expected by superheating the pool 100 to 200°C. Experience with e-beam melting Ti ingots show the following dependence of the pool temperature on beam power. (Figure 6).⁽¹⁶⁾

Present day commercial furnaces may show a vacuum better than that estimated from the ingot analyses (2.5×10^{-4} torr). However another important aspect of the problem is that equilibrium may not be reached in one or two melts or in the fast melting rate used in industrial production. Multiple melts or slower melts could be essential to reach the equilibrium concentrations given by the equations in Table 4. At Fansteel⁽¹⁷⁾ melting an ingot 8 times in a vacuum $\sim 1 \times 10^{-4}$ torr allowed the top to reach an RRR of 90.⁽⁴⁾ One additional slow melt of part of this ingot in a furnace at AMES* laboratory at a vacuum $\approx 10^{-5}$ torr improved the RRR to 165, close to the calculated equilibrium value. Many years ago, Smith⁽¹⁸⁾ achieved the following impurity reduction with multiple melting (Table 6). Both Wah Chang⁽¹⁹⁾ and Hereaus⁽²⁰⁾ have recently reported similar capabilities.

Improvements can also be expected from optimizing other melt conditions; for example larger diameter ingots would increase the surface area of the molten pool. In this direction the alternate furnace design called the e-beam cold hearth furnace⁽²¹⁾ could be very effective (Figure 7). This design provides maximum exposure of the melt to the vacuum environment by melting in a rectangular hearth and at the same time casting a slab shape, more suitable for rolling than the round ingot, as I shall discuss later. A disadvantage is that the large area of contact to the cooling water leads to high losses which must be compensated by additional power with more electron guns placed along the length of the hearth.

One problem sometimes observed with e-beam melted ingots is the nonhomogeneous distribution of impurities.⁽⁴⁾ Variations in the gaseous content of the raw material could persist in the final product. Scrambling the raw material is a possible remedy. The skin of the ingot has been found to contain more impurities than the interior. A slice from the Fansteel ingot mentioned earlier was

* F. Schmidt, AMES Laboratory, Iowa State University, Ames, Iowa 50011

dissected into many pieces and the RRR measured.⁽⁴⁾ (See Figure 7) Top to bottom inhomogeneity has also been observed. The first part of the melt which usually ends up at the bottom getters the vacuum system in the early stages of the melt. Machining away the "bark" and cutting away a short section from the bottom are recommended for a purer final product.

After a satisfactory ingot is cast the first step is usually to forge the ingot into a rectangular slab of thickness and width appropriate to fit inside the rolling mill. Some manufacturers pursue hot forging (900 - 1100°C) at atmospheric pressure to facilitate working and avoid cracking due to the large grains present. This procedure produces a thick oxide scale which is machined away. If possible, hot forging should be avoided to reduce the risk of contamination. Evidence in the literature⁽²²⁾ shows that Nb free from interstitials has a lower yield point, (Figure 9) so that cold forging should be possible with improved purity. Fansteel successfully cold forged an 8" diameter by 6 ft long ingot (average RRR = 70) to a 2.6 x 8" rectangular slab, over a factor of 2 cross-sectional area reduction.

After forging, the slab is annealed at a temperature high enough to give near 100% recrystallization (1000 - 1200°C), rolled to an intermediate thickness (~ 0.5"), annealed, rolled to the final sheet thickness and then final annealed to yield grains ~ 50 μm diameter with near 100% recrystallization.

Choosing the proper annealing conditions is important to produce the correct grain size, near 100% recrystallization and highest possible RRR. The recrystallization temperature depends on the impurity content and sets the minimum temperature. The % recrystallization depends on the amount of cold work and increases with annealing temperature. Success in achieving a high RRR depends on avoiding further contamination during the anneal. The diffusion lengths of O, N and C in one hour are given in Table 7 along with the diffusion coefficients.⁽²³⁾ The amount of O pickup above 1100°C for a thin sheet is approximated by⁽²⁴⁾

$$\Delta C(\text{at } \%) = \frac{1.29}{1 + 1.3 \times 10^{-2} \exp \left(\frac{7150}{T} \right)} \times \frac{F}{V} (\text{cm}^{-1}) \times P_{\text{O}_2} (\text{torr}) \times \epsilon (\text{sec})$$

$\frac{F}{V}$ is the surface area to volume ratio

At 1100°C and 10^{-6} torr oxygen partial pressure, a 2 mm sheet will pick up 23 wt ppm of O, which impurity, if present alone, would limit the RRR to 217. Once again a good vacuum ($p < 10^{-6}$ torr) is essential during the final anneal. Later I shall mention a way to protect the Nb during final anneal if the pressure is higher.

During rolling, many dislocations are produced which also lower the RRR. Rolling a section of 2" ingot to 0.062" thickness (97% deformation) lowered the RRR from 165 to 110 showing that if the dislocations were present alone the RRR would be 350. Thus dislocations produce a significant but minor contribution to the electron scattering.²⁵

III. Post Production Purification

The post purification methods may be classified into two categories,

- (1) UHV, high temperature degassing,
- (2) solid state gettering.

For (1) the relevant outgassing relationships were given earlier in discussing purification during e-beam melting. However, for structural reasons the post purification temperatures need to be held several hundred degrees lower than the melting point. To make any gain in removal of O and N, UHV conditions become essential, i.e., $p < 10^{-7}$ torr. Table 8 shows the residual O and N content at 1900 and 2000°C for pressures of 10^{-8} and 10^{-7} torr. The pressures must be at these excellent levels in the hot zone. Unfortunately this is found not to be the case in high temperature UHV furnaces used for firing cavities, eg. at HEPL, KFK, BNL and Wuppertal. These furnaces usually increase the O content. In Table 9, chemical analyses as well as RRR measurements are presented for Nb samples fired at 2000°C in BNL and KFK furnaces at nominal pressures between 10^{-8} and 10^{-7} torr as measured by the ion pump current.⁽²⁶⁾

The low pressures required can be achieved in furnaces where the part to be degassed is the only hot element and very efficient pumping arrangements that avoid excessive baffling by radiation shields are used. These methods have been used at MPI to obtain $RRR > 10^4$ in Ta free Nb.⁽³⁾ At Cornell we have degassed χ -band elliptical cavities at 2000°C by resistive and induction

heating of the cavities in an ion pumped vacuum chamber. RRR values up to 1200 were obtained. The main disadvantage of these methods is that at the high temperature necessary, large structures creep and deform under their own weight or due to pressure exerted by supporting fixtures.

Conditions for removal of carbon are more favorable. Heating between 1650 and 1800°C in an oxygen atmosphere of 10^{-6} torr is usually sufficient.⁽¹⁵⁾ However the decarburization usually increases the O content, so it becomes necessary to follow up with a high temperature UHV degassing. Removal of H is the easiest.⁽¹⁵⁾ Heat treatment above 800 C in a moderately good vacuum ($p < 10^{-5}$ torr) is effective in reducing H to below 1 wt ppm.

Solid state gettering is a process whereby a metal which has a higher affinity to O (or N and C) is brought into contact with Nb and acts as a sink for interstitial diffusion of impurities.⁽²⁷⁾ The technique has been applied in the past largely to Vanadium using Ti⁽²⁸⁾ and Zr⁽²⁹⁾ or sinks and to a lesser extent to Nb⁽³⁰⁾ using Zr as a sink.

At Cornell we have developed this process using a vapor deposited Yttrium (Y) film on the Nb surface.⁽³¹⁾ Nb sheet, or cavity half shells or a finished cavity is wrapped loosely in Y foil. In practice it is convenient to capture the Y foil within two layers of perforated sheet Nb and place the composite in close proximity to the surface of the part undergoing purification (Fig. 10). Direct contact with Y foil is avoided to facilitate the clean up of the Y film. The assemblage is heated to 1250°C in a vacuum of 10^{-5} torr or better for 4 hours. At this temperature the vapor pressure of Y is 1.7×10^{-5} torr⁽³²⁾ so that several μm of Y are deposited on the Nb surface. The Y, which has a higher affinity to O than does Nb, traps the O diffusing rapidly from the bulk to the surface. The diffusion length of) at 1250°C is 1.4 mm per hour so that removal in 4 hours is very effective. During the heating cycle the impurity atoms from the furnace vacuum are also intercepted by the Y coating and prevented from further contaminating the Nb. After purification, the Y layer is dissolved in HNO_3 followed by a 1 minute etch in standard buffered chemical polish used for Nb cavity processing.

Solid state gettering by Y offers several technical advantages over UHV high temperature outgassing. Lower purification temperatures allow complicated structures to be treated without risk of deformation. Less stringent vacuum conditions are possible due to the protective nature of the film.

By application of this process, the RRR of commercial grade Nb improved from 25 to between 80 and 100 and of multiple e-beam melted Nb from between 60 to 80 to between 310 and 360.^(4,31) Y-treatment applied to multiple electron beam melted Nb supplied by AMES Laboratory improved from 165 to 540.

The effectiveness of Y is superior to that of Ti or Zr.⁽³¹⁾ The vapor pressure of Y is almost 10 times higher than that of Ti and almost 10^6 times higher than Zr, allowing sufficiently thick coatings. Both Zr and Ti have substantial solid solubilities in Nb whereas Y has none,⁽³³⁾ reducing the possibility of contamination. Figure 11 compares the effectiveness of Y with Ti and Zr. Commercial grade Nb (thickness 1.5 mm) improved in RRR from 20 to 29 in 1 hour at 1250 using Ti and to 76 in the same time at the same temperature using Y. A comparison between Y and Ti at the same vapor pressure instead of the same temperature also shows Y superior. At 1160°C the vapor pressure of Y is the same as that of Ti at 1250°C; however with Y the RRR is 50 compared to 29 with Ti. Ti is however, considerably less expensive than Y so that using it for longer times and at higher temperatures can yield RRR improvements comparable to Y⁽³⁴⁾ but with risk of increased Ti contamination, (Fig. 12).

IV. Conclusions

There is much room for improvement over commercial grade Nb and several possible techniques have been discussed to bring about these needed improvements. Some of these techniques have already been applied by industrial Nb suppliers. RF cavity builders need no longer use Nb with RRR of 20 - 30 since Nb with RRR's between 80 - 120 is now available. The solid state gettering technique, developed at Cornell, should eventually find its way to industrial application as the need for even purer Nb arises. This technique allows yet another factor of ~ 3 improvement in conductivity over and above that realizable by multiple electron beam melting. Thus it should soon be possible to obtain sheet material with RRR's as high as 500, by improving melt conditions and following up with gettering.

It is important to keep in mind a disadvantage of higher purity Nb for rf cavities. Fig. 13 shows the BCS surface resistance vs. the mean free path

of Nb for several frequencies.⁽³⁵⁾ Very roughly the surface resistance increases as the fourth root of the mean free path. Already at RRR's of 100, the BCS Q decreases by ~ 40 - 50% as has been observed with 1500 Mhz cavities at Cornell. For cavities designed to operate in the BCS resistance regime (i.e., 4.2K) this drop in Q_0 would constitute an important additional refrigerator load.

The beneficial effects of thermal conductivity improvements on cavity field levels are already forthcoming. Table 10 shows the recent best results on cavities made from high RRR Nb at Cornell, CERN and Wuppertal.

In 1972 J. Turneure⁽³⁷⁾ reviewed the maximum surface magnetic fields obtained in a number of cavities over a frequency range including 1.3 Ghz to 10.5 Ghz and plotted the results as a function of cavity area. The dashed curve in Fig. 14 is approximately the upper limit of the best results obtained at the time. At about the same period, P.B. Wilson⁽³⁸⁾ proposed a statistical model for breakdown. He characterized defects by the fraction r of the critical field at which they breakdown, and assumed a defect distribution that rises sharply around $r_1 H_c$ ($H_c = 1500$ Gauss, $r_1 = 0.6$). The sharpness of the rise was chosen as $(r/1-r)^\alpha$ with $\alpha = 3$. From these considerations, the area dependence of the breakdown field level was found to be nearly $A^{-1/4}$, which is plotted as the solid line in Figure 14 and agrees well with upper limit to the 1972 data as represented by Turneure. Since their inception in 1978, a lot of data on spherical and elliptically shaped cavities has been accumulated in a number of laboratories over a wide frequency (and area) range from 350 Mhz to 8600 Mhz, in single as well as multi-cell structures. Remarkably, when these new data are plotted as a function of cavity area, the best results once again fall (mostly) under the Turneure-Wilson limit. Most "guided-repair" cavity results also fall under this line. However, the higher thermal conductivity cavity data clearly breakthrough the statistical limit, especially in the large area cavities. The expectations of field level increases with thermal

conductivity are indeed being realized.

Acknowledgements

It is a great pleasure to acknowledge the many informative discussions with colleagues at Cornell, CERN and Wuppertal. The cooperation of R. Droegkamp at Fansteel Co., and F. Schmidt at AMES Laboratory in producing high RRR Nb is appreciated.

Table 1 - The Effect of Impurities on the RRR of Niobium

<u>Element</u>	<u>RRR for 1 wt ppm</u>
O	5000
N	3900
C	4100
H	1550
Ta	550,000

Table 2 - Impurity Analyses Techniques

<u>Method</u>	<u>Elements Determined</u>	<u>Lower Limit of detection</u>
Emission Spectrometry	Metallic	1 - 10 ppm
Spark Mass Spectrometry	All	3 ppb - 300 ppb
Laser Mass Spectrometry	C, O, N, H	~ ppb
Activation Analysis	Most	1 ppb - 100 ppm
Vacuum fusion, Hot	O, H, N	0.1 - 10 ppm
Vacuum Extraction, Inert		
Gas Fusion		
Combustion	O, C	1 - 10 ppm
Kjeldahl	N	1 - 10 ppm

Table 3 - A comparison between measurements of O, N, C concentrations by classical methods and RRR measurements.

		<u>Fansteel</u>								
O	115	30	48	70	114	32	10			
N	10	21	17	34	10	10	14			
C	<10	<10	<10	20	<10	<10	<10			
RRR _C	37(C=5)	80(C=5)	66(C=5)	36	38(C=5)	98(C=5)	148(C=5)			
RRR _M	32	82	75	49	36	102	86			
% discrepancy w.r.t. measured value	16	2	12	26	6	4	72			
		<u>Ledoux*</u>								
O	107	50	45	18	28	122	96	95	152	136
N	54	50	18	12	18	44	21	41	32	33
C	3	4	ND	2	14	16	<5	8	5	<5
RRR _C	28	43	74	104	71	25	41(C=0)	32	25	28
RRR _M	27	62	68	175	74	20	46	40	28	25
% discrepancy w.r.t. measured value	4	30	9	40	4	25	11	20	11	12

Table 3 (cont.)

	<u>KBI</u>	
O	126	130
N	74	76
C	4	14
RRR _C	22	21
RRR _M	19	29
% Discrepancy w.r.t. measured value	16	28

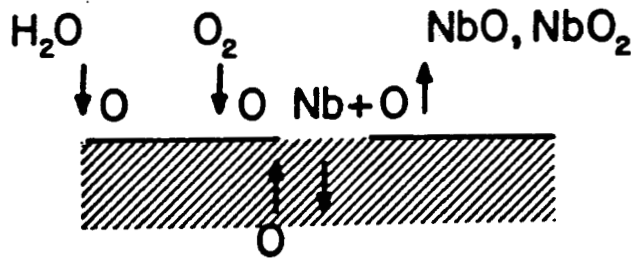
	<u>AMES Lab</u>				
O	31	7	16	13	4
N	9	9	6	8	4
C	15	1	7	1	<2
RRR _C	82	256	155	206	434
RRR _M	~100	162	165	178	165
% Discrepancy w.r.t. measured value	14	58	6	16	163

RRR_C = Calculated RRR

RRR_M = Measured RRR

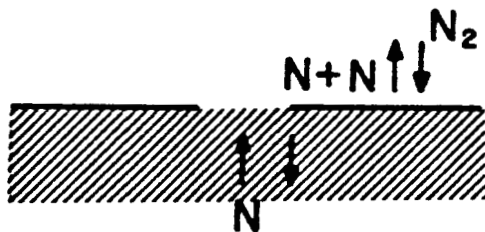
*Ledoux & Co., Teaneck, NJ 07666

Table 4 - Outgassing reactions and equations for Nb.

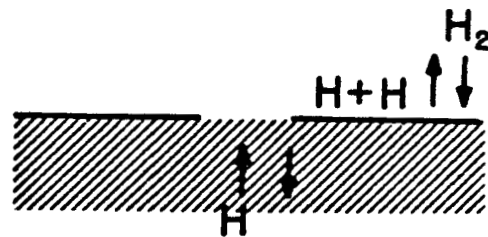


$$C_O = 2.1 \times 10^{-4} P_{O_2} \exp(60410/T)$$

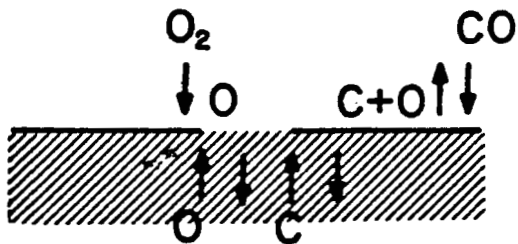
$$C_O = 1.48 \times 10^{-2} P_{H_2O} \exp(45200/T)$$



$$C_N = 0.94 \sqrt{P_{N_2}} \exp(23150/T)$$



$$C_H = 0.38 \sqrt{P_{H_2}} \exp(4200/T)$$



$$C_C = 1.07 \frac{P_{CO}}{C_O} \exp(33600/T)$$

$P_{O_2}, P_{N_2}, P_{CO}, P_{H_2O}$ in torr

T in ° Kelvin

$C_H, C_O, C_N,$ and C_C in wt ppm

Table 5 - Effect of superheating molten pool on the purity of a Nb ingot.

Partial pressure = 1×10^{-5} torr each of O_2 , N_2 and Co .

$\frac{\Delta T}{^\circ C}$	$\frac{O}{ppmw}$	$\frac{N}{ppmw}$	$\frac{C}{ppmw}$	$\frac{RRR(O+N)}{}$
0	9	14.5	$2.4/C_o$	184
+100	4.1	10.8	$1.6/C_o$	284
+200	2	8.2	$1/C_o$	488

Partial Pressure = 1×10^{-4} torr each of O_2 , N_2 and CO

$\frac{\Delta T}{}$	$\frac{O}{}$	$\frac{N}{}$	$\frac{C}{}$	$\frac{RRR(O+N)}{}$
0	90	45.8	$24/C_o$	34
+100	41	34.2	$16/C_o$	60
+200	20	25.9	$10/C_o$	96

Table 6 - Multiple e-beam melting Nb - analysis ppm weight eight. (18)

	<u>Starting Material</u>	<u>1st Melt</u>	<u>2nd Melt</u>	<u>3rd Melt</u>
O	894	580	95	18
N	580	64	20	15
C	460	---	40	30
RRR _{calculated}		<7	29	67

Table 7 - Diffusion Coefficients⁽²³⁾ and diffusion lengths for O, N and C in Nb.

O:	$.02 \exp(-1.354 \times 10^4/T) \text{ cm}^2/\text{sec}$
C:	$.0043 \exp(-1.670 \times 10^4/T) \text{ ''}$
N:	$.0085 \exp(-1.758 \times 10^4/T) \text{ ''}$

<u>T</u> (c)	<u>O</u> mm/hr	<u>N</u> mm/hr	<u>C</u> mm/hr
900	0.4	0.005	0.005
1000	0.6	0.008	0.008
1100	0.9	0.13	0.13
1200	1.2	0.19	0.19
1400	2.0	0.38	0.38

Table 8 - Equilibrium concentrations for O and N due to UHV outgassing Nb at high temperatures.

P T	10^{-8} torr		10^{-7} torr	
	1900	2000	1900	2000
O	4	1.1	40	11
N	4	2.5	12.6	7.9
RRR Calculated	555	1183	90	240

Table 9 - Effect of Firing Nb in KFK, BNL and HEPL UHV furnaces customarily used for firing SC Cavities.

Treatment	O	N	C	RRR _m	RRR _C
As received	95	41	8	40	32
Fired at KFK, 2000°C 10^{-8} torr	152	32	5	28	25

As Received	31	9	15	86	80
Fired at 2000°C at KFK 10^{-8} torr	136	33	5	25	28

As received	31	9	15	79	80
Fired at 2000°C, HEPL 5×10^{-7} torr	--	--	--	71	--

As received	48	17	<10	72	75
Fired at 2000°C, BNL 10^{-7} torr	114	10	<10	36	39

Table 10 - Recent best results on improved thermal conductivity cavities

Laboratory	Frequency (Mhz)	Cavity	RRR	Method	E_{acc}^{max} MV/m	H_{peak} Gauss	E_{peak} MV/m
Cornell	1500	1 cell elliptical	~80	Y treat- ment	18.2 ⁺ 13.3*	850	34
Cornell	1500	5 cell w/ couplers	~80	Y treat- ment	15.3	715	39
CERN ³⁶	500	1 cell spherical	112	Multiple melts (Hereaus)	13.9	528	29
Wuppertal ³⁶	3000	1 cell spherical	135	Multiple melts (Hereaus)	16	672	41

+ 5 cell equivalent accelerating field if limited by thermal breakdown.

* 5 cell equivalent accelerating field if limited by field emission.

REFERENCES

1. The Scanning Laser Acoustic Microscope (SLAM) is a new analytical instrument which produces magnified images of the internal features of a sample using high frequency ultrasonic waves.
 - a. L. W. Kessler and D. E. Yuhas, "Acoustic Microscope - 1979", Proc. IEEE, Vol. 67, No. 4, April 1979, pp. 526-536.
 - b. L. W. Kessler and D. E. Yuhas, "Principles and Analytical Capabilities of the Scanning Laser Acoustic Microscope (SLAM)", SEM/1978, Vol 1, pp. 555-560 (April 1978).
 - c. L. W. Kessler, "A Review of Progress and Applications in Acoustic Microscopy", J. Acoustic Society America 55, pp. 909-918 (1974).
 - d. D. E. Yuhas and T. E. McGraw, "Acoustic Microscopy, SEM, and Optical Microscopy: Correlative Investigations in Ceramics", Proc. Scanning Electron Microscopy, 1979 I, SEM, Inc. AMR O'Hare, IL 60666, pp. 103-110.
2.
 - a. H. Padamsee "Calculations for Breakdown Induced by 'Large Defects' in Superconducting Nb Cavities", IEEE Trans. Mag-19, 1322 (1983), and CERN/EF/RF,- 82-5.
 - b. H. Padamsee and R Kahn, "Additional Thermal Model Calculations for High RRR Nb Cavities", SRF-840403, Cornell University, LNS Internal Report, (1984).
 - c. H. Padamsee, "Influence of Thermal Conductivity on the Breakdown Fields of Niobium Cavities", 1984 Applied Superconductivity Conference, to be published.
3. K. K. Schulze, "Preparation and Characterization of Ultra-High Purity Niobium", Journal of Metals, 33, May 1981.
4. H. Padamsee, R. Droegkamp and K. Jensen, "Production of High Resistivity Ratio Niobium Sheet by Fansteel Company", SRF-840401, Cornell University LNS Internal Report.
5. L. P. Kadanoff and P. C. Martin, "Theory of Many-Particle Systems II, Superconductivity", Phys. Rev. 124, 670 (1961).
6. N. W. Ashcroft, and N. D. Mermin, Solid State Physics, Holt, Rinehart and Winston, NY 1976.
7. W. M. Henry and E. R. Blosser, "Brief Survey of Various Analytical Techniques used for Metals and Alloys", Techniques of Metals Research, Vol III, part 1, pp. 1, Ed. R. F. Bunshah, Interscience, John Wiley & Sons, 1970.
8. V. G. Mossotti, "Emission Spectroscopy Including dc Arc, Spark, and other Methods", in Techniques of Metals Research, Vol. III, part 2, p. 533, Ed. R. F. Runshah, Interscience Publishers, John Wiley & Sons (1970).
9.
 - a. R. E. Honig, "Mass Spectrometric Techniques", in Techniques of Metals Research, Vol. III, part 2, Ed. R. F. Runshah, Interscience Publishers, John Wiley & Sons (1970).

References (cont.)

- b. W. L. Harrington, R. K. Skogerbee and G. H. Morrisson, "Quantitative Spark Source Mass Spectrometry Using Cryosorption Pumping", *Anal. Chem.*, 37, 1480 (1965).
- z c. W. L. Harrington, R. K. Skogerbee and G. H. Morrisson, "Determination of Trace Amounts of C, O, and N in Metals by Spark Source Mass Spectrometry", *Anal. Chem.*, 38, 321 (1966).
10. a. P. Albert, "Activation Analysis with Thermal Neutrons", p. 687;
b. J. Laverlochere, "Activation Analysis with Fast Neutrons", p. 755;
c. C. H. Englemann, "Activation Analysis with Gamma Rays and Charged Particles", p. 777, above in Techniques of Metals Research, Vol. III, part 2, Editor R. F. Bunshah, Interscience Publishers, John Wiley & Sons, (1970).
11. Z. Shankai, R. J. Conzemius and H. J. Svec, "Determination of Carbon, Nitrogen and Oxygen in Solids by Laser Mass Spectrometry", *Anal. Chem.* 56, 382 (1984).
12. M. W. Mallet and S. Kallamann, "Vacuum Fusion, Vacuum Extraction and Inert Gas Fusion Techniques", p. 69, in Techniques of Metals Research, Vol III, pt.1.
13. W. G. Boyle, "Combustion Methods for Carbon and Sulphur", p. 115 in Techniques of Metals Research, Vol. III, part I, ed. R. F. Bunshah, Interscience Publishers, John Wiley & Sons (1970).
14. R. F. Bunshah and M. A. Cocca, "Electron Beam Melting, Annealing and Distillation Techniques", p. 717 in Techniques of Metals Research, Vol 1, part 2, ed R. F. Bunshah, Interscience Publishers, John Wiley & Sons (1970).
15. a. K. Schulze and H. Jehn, *Z. Metall Kunde* 68, 654 (1977);
b. J. R. Cost and C. A. Wert, "Metal-Gas Equilibrium in the Niobium-Nitrogen Terminal Solid Solution", *Acta Metallurgica* 11, 21 (1963);
c. E. Veleckis and R. K. Edwards, *J. Phys. Chem.* 73, 683 (1969);
d. E. Fromm and G. Spaeth, *Z. Metallkunde* 59, 65 (1968);
e. E. Fromm and H. Jehn, "Stationare Zustände beim Glühen von Niob und Tantal in Wasserdampf", *Z. Metallkunde* 58, 120 (1967).
16. R. F. Bunshah and R. S. Juntz, Trans. Vacuum Met. Conf., 1965, Am. Vacuum Soc., Boston, MA p. 200.
17. Fansteel Metals, 1 Tantalum Place, N. Chicago, IL 60064.
18. H. R. Smith, Trans. Vacuum Met. Conf., 1962, Am. Vacuum Soc., Boston, MA, p. 95.

References (cont.)

19. Teledyne Wah Chang Albany, Albany, OR 97321.
20. W. C. Hereaus BmbH, D-6450 Hanau 1, W. Germany.
21. C. d'A Hunt and H. R. Smith, *J. Metals*, 18, 570 (1966).
22. R. E. Reed, "Electron Beam Floating-Zone Refining of Niobium", Second Int'l Conf. on Electron and Ion Beams in Science and Technology, Gordon & Breach, NY (1969).
23. R. W. Powers and M. V. Doyle, "Diffusion in Group V Transition Metals", *J. Appl. Phys.* 30 514 (1959).
24. a. G. Horz, "Mechanisms and Kinetics of Absorption and Desorption Reactions in Systems of Refractory Metals with Nitrogen, Oxygen or Carbon", *Metall. Trans.* 3, 3069 (1972).
b. G. Horz, *Z. Metallkunde*, 59, 283 (1968).
25. R. B. Zubeck, T. W. Barbee, T. H. Geballe and F. Chilton, "Effects of Plastic Deformation on the Superconducting Specific Heat Transition of Niobium", *J. Appl. Phys.* 50, 6423 (1979).
26. a. H. Padamsee and D. Sessko, "Materials Characterization of Commercial Grade Niobium", SRF 830505, Cornell University, LNS Internal Report, (1983).
b. H. Padamsee, F. Palmer and D. Sessko, "Materials Characterization of AMES Supplied Niobium", SRF 830504, Cornell University, LNS Internal Report, (1983).
27. R. Kirchheim, "Metals as Sinks and Barriers for Interstitial Diffusion with Examples for Oxygen Diffusion in Copper, Niobium and Tantalum", *Acta Metallurgica*, 27, 869 (1979).
28. D. T. Peterson, B. A. Loomis and H. H. Baker, "Purification of Vanadium by External Gettering", *Metall. Trans.* 12A, 1127 (1981).
29. O. Yohinari, T. Konno, K. Suma and M. Koiwa, "Solid State Deoxygenation of Vanadium", *J. Less Common Metals*, 81, 239 (1981).
30. K. Shibata and M. Koiwa, "The Effect of Hydrogen and Deuterium on the Internal Friction of Deformed Niobium", *Trans. Japan. Institute of Metals*, 21, 639 (1980).
31. a. H. Padamsee, "Purification of Niobium", U. S. Patent Application No. 594, 592 (Pending).
b. H. Padamsee, "A Low Temperature, Intermediate Vacuum Process for Removing Oxygen Impurity from Niobium", SRF 830902, Cornell University, LNS Internal Report (1983).

References (cont.)

- c. H. Padamsee, "A New Purification Technique for Improving the Thermal Conductivity of Superconducting Nb Microwave Cavities", 1984 Applied Superconductivity Conference, (to be published).
32. AIP Handbook, 3rd Edition, p. 4-300, McGraw-Hill (1972).
33. F. A. Shunk, Constitution of Binary Alloys, Second Supplement, McGraw-Hill.
34. P. Kneisel, "Some Preliminary Results on the Degassing of Niobium with Titanium", SRF 840702, Cornell University, LNS Internal Report (1984).
35. J. Halbritter, "Comparison between Measured and Calculated RF Losses in the Superconducting State:", Z. Physik 238, 466 (1970).
36. H. Piel, Proc. of the 1984 Linear Accelerator Conference, Darmstadt, West Germany (1984).
37. J. P. Turneaure, "The Status of Superconductivity for RF Applications", Proc. of the 1972 Applied Superconductivity Conference, Annapolis (1972) IEEE Pub. No. 72 CH0682-5-TABSC.
38. P. B. Wilson, "Current Status of Superconductor Accelerator Technology", SLAC-PUB-1134 (ACC) (1972).

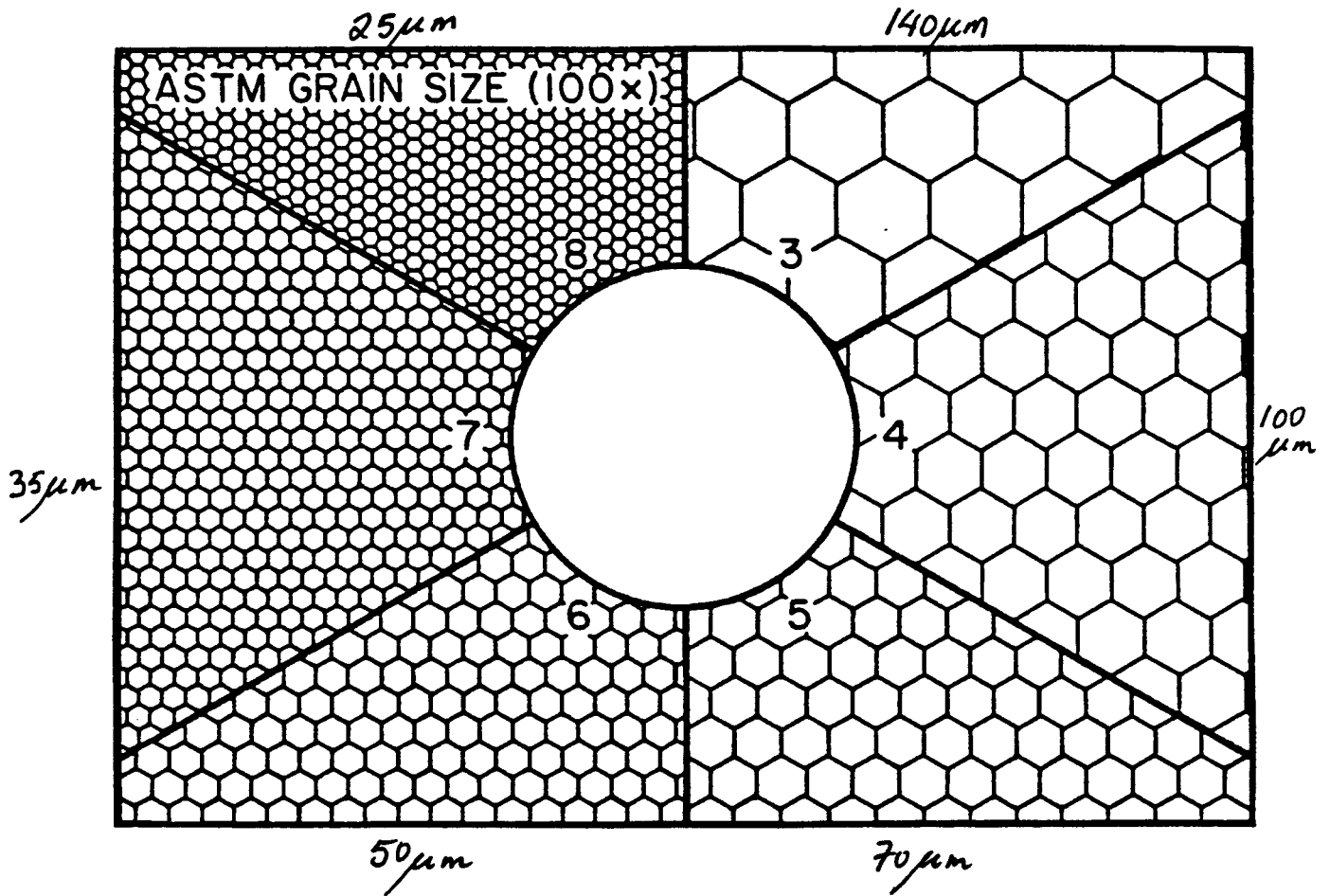


Fig. 1. ASTM grain sizes 3 to 8, 100 x magnification.

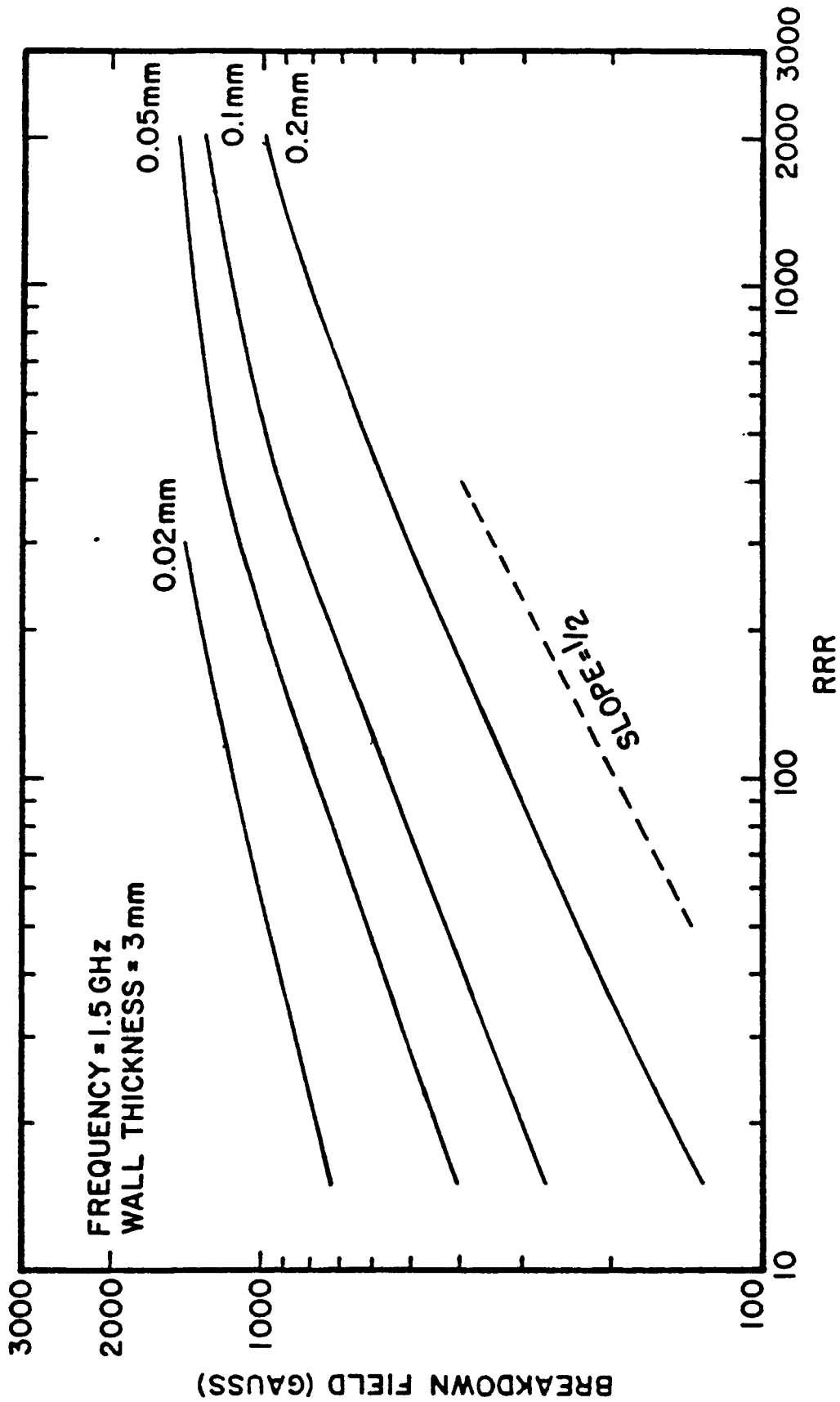
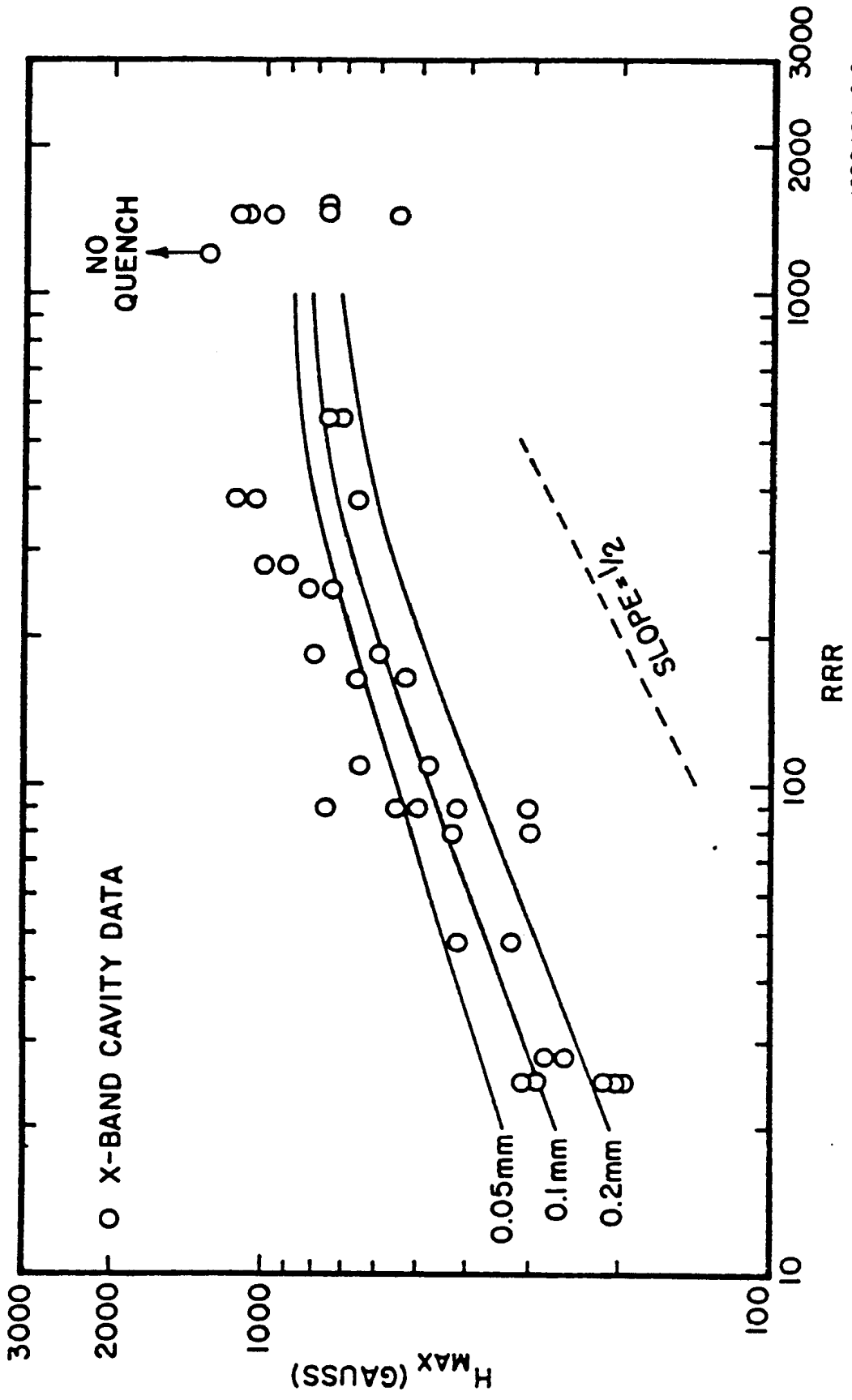


Fig. 2. (a) Breakdown field vs RRR for different defect sizes. A constant defect resistance of 8×10^{-3} ohms is chosen, frequency = 1.5 GHz, wall thickness = 3 mm.



1620484-010

Fig. 2. (b) $f = 8.6$ Ghz, wall thickness = 0.5 mm; data points shown are for X-band elliptical cavities measured at Cornell.

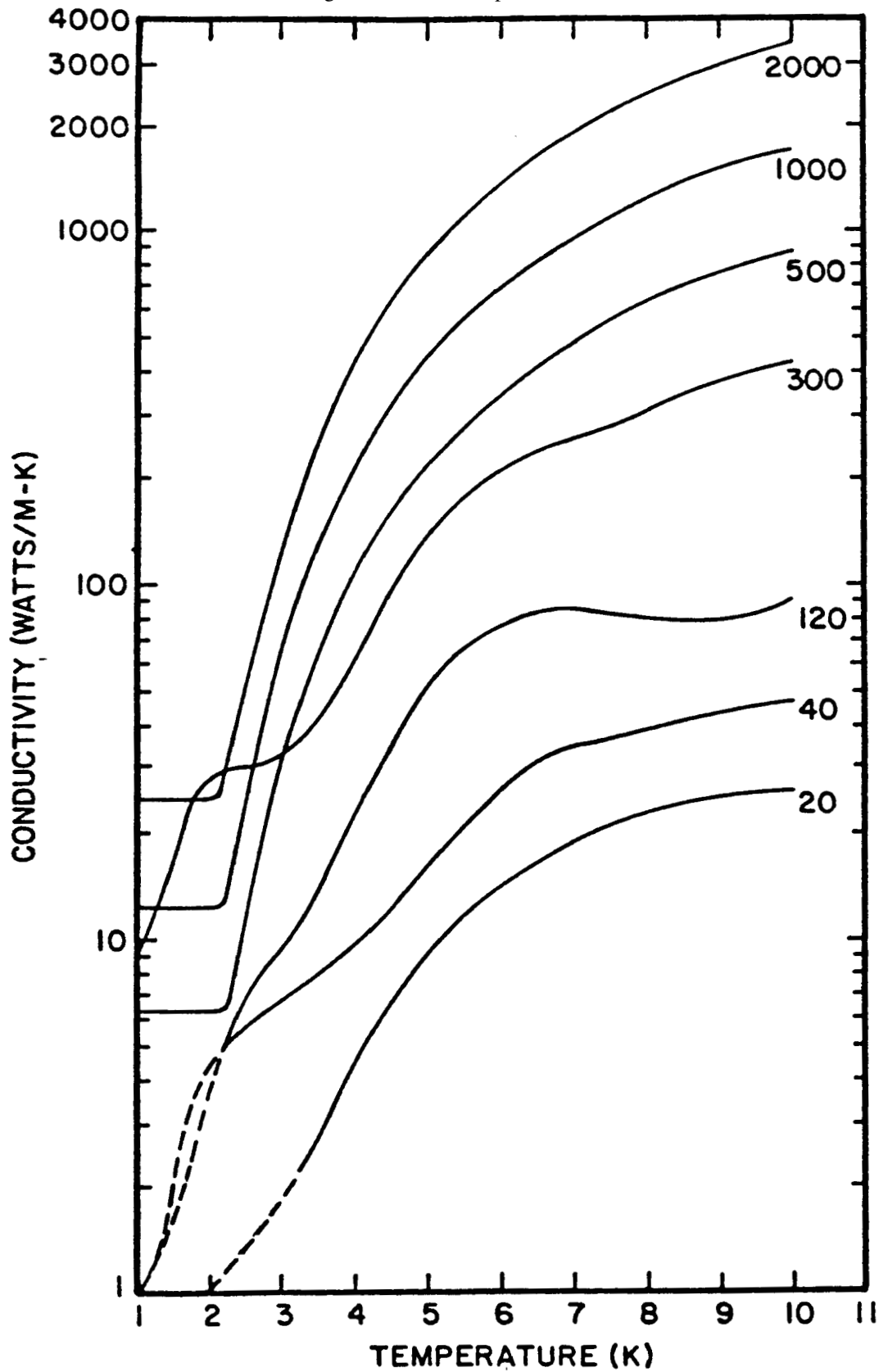
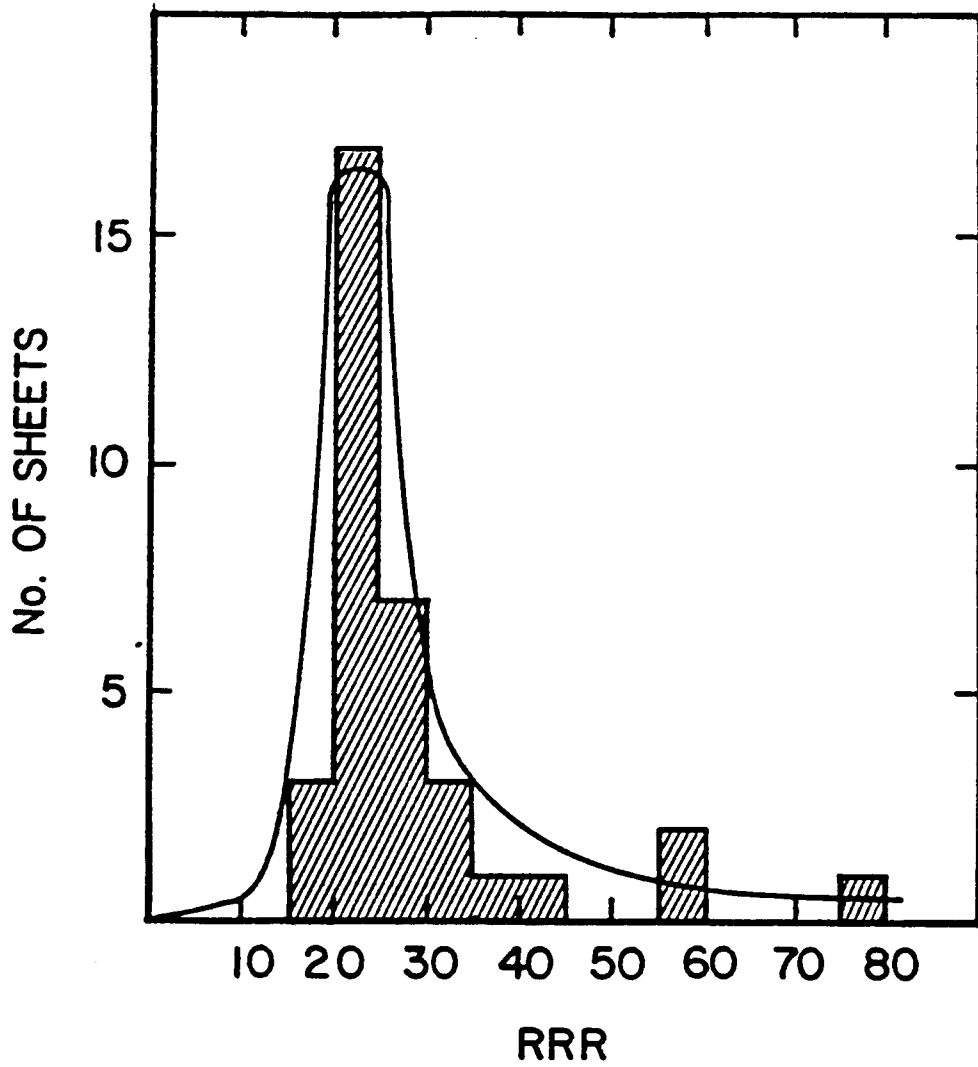


Fig. 3. Thermal conductivity functions used in the calculations. The numbers next to each curve are the RRR values.



1620484-002

Fig. 4. Distribution of RRR for Commercial Nb sheet stock at Cornell.

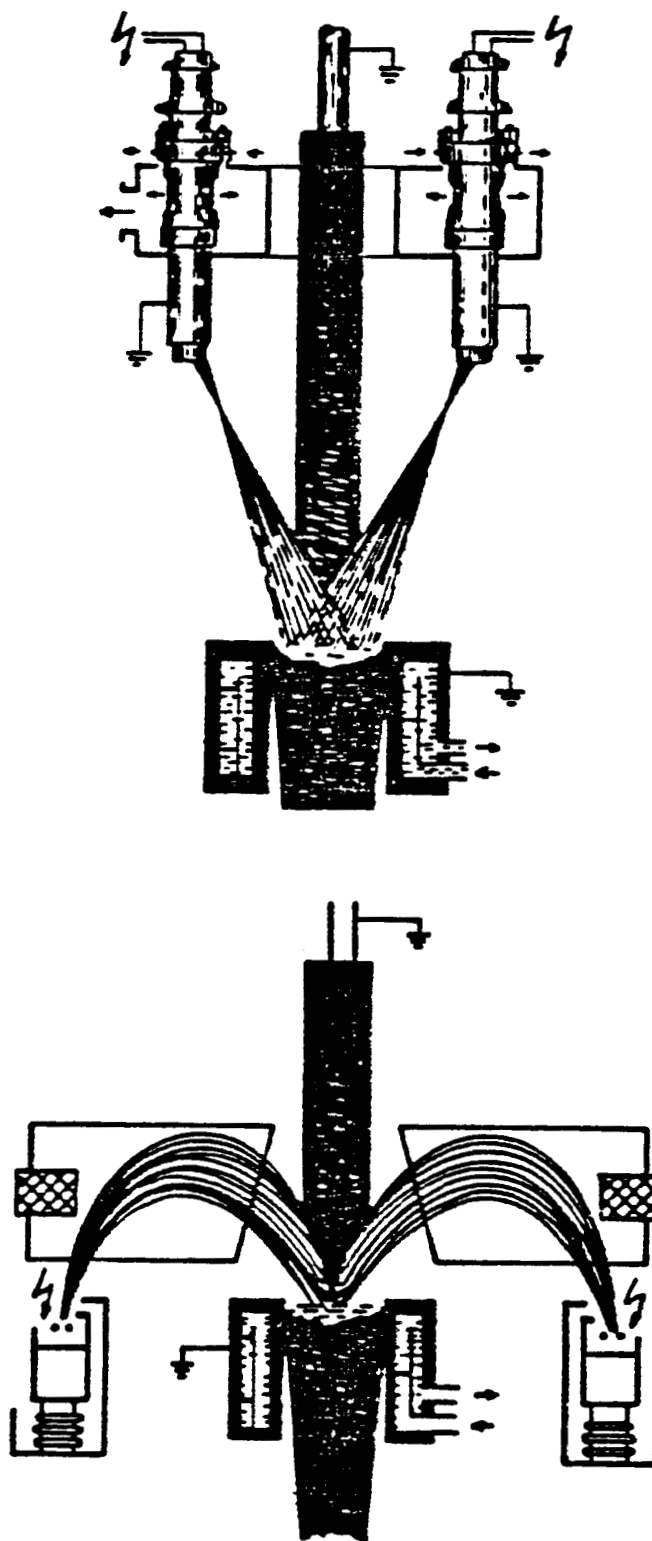


Fig. 5. Schematic for two types of electron beam furnaces for melting Nb ingots.

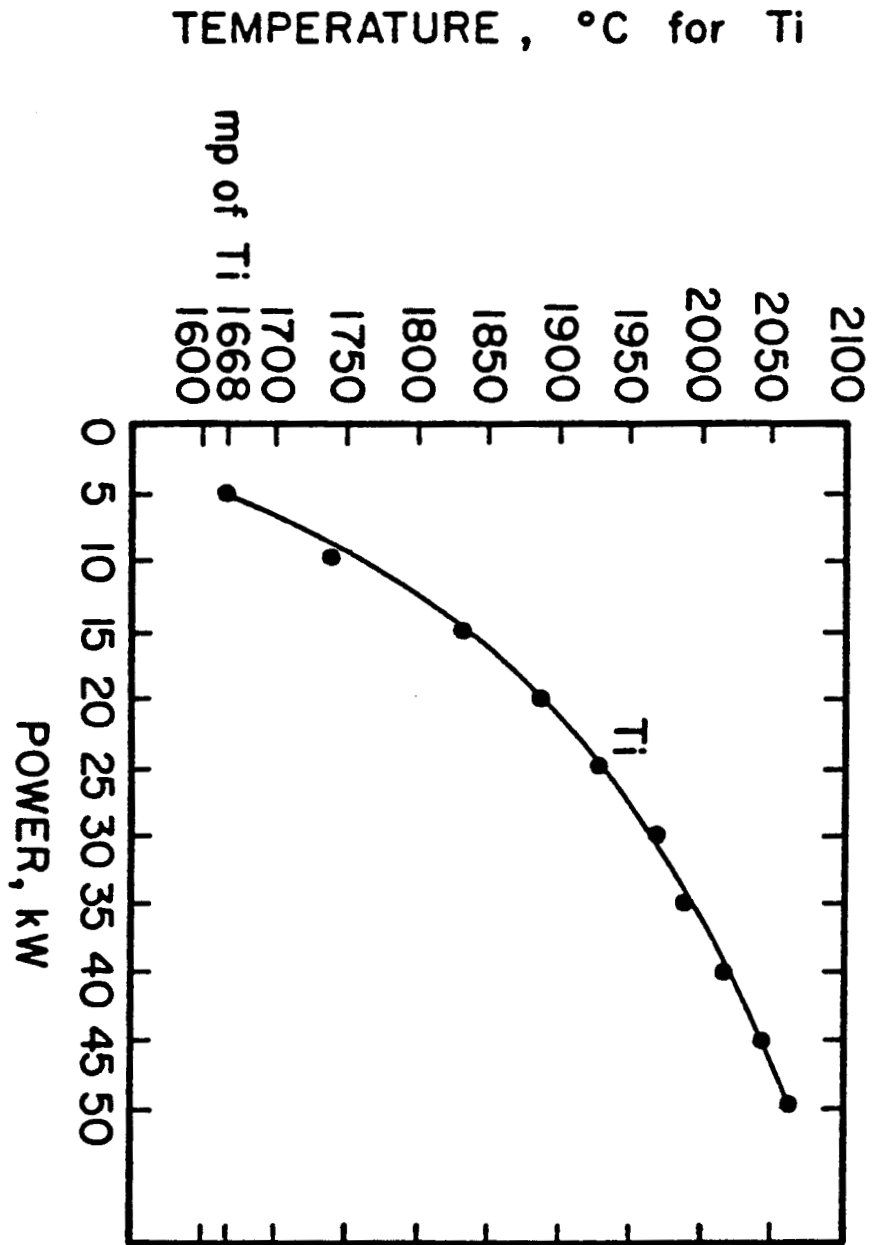


Fig. 6. Electron beam power required for superheating Titanium ingots.

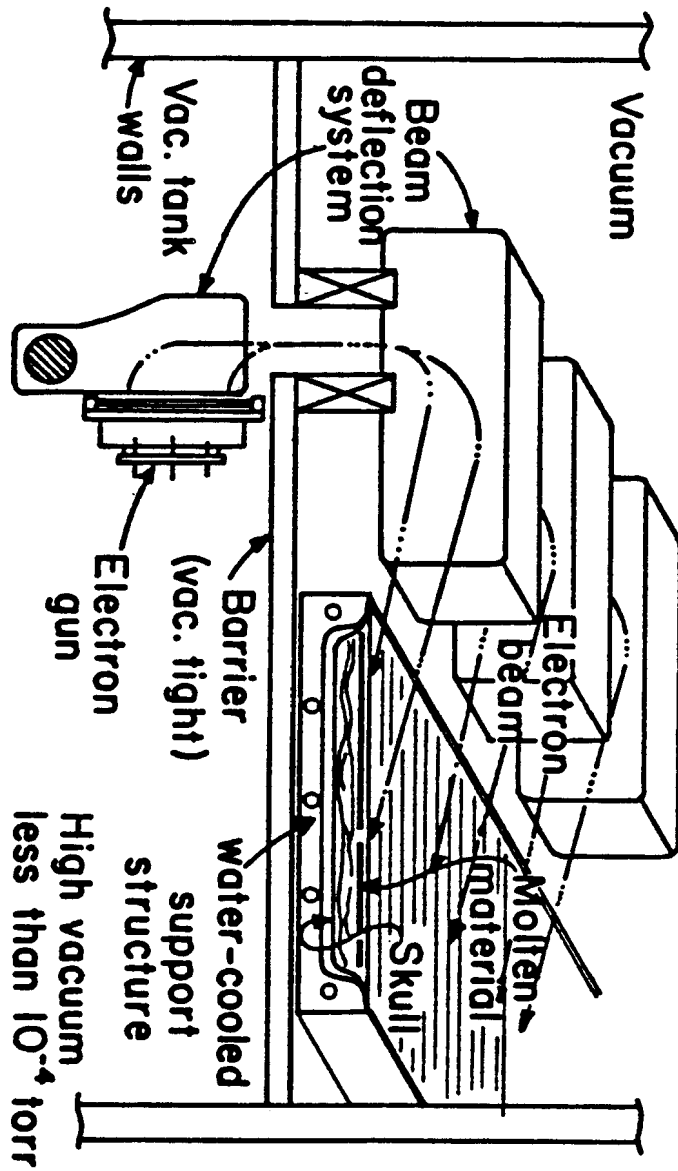
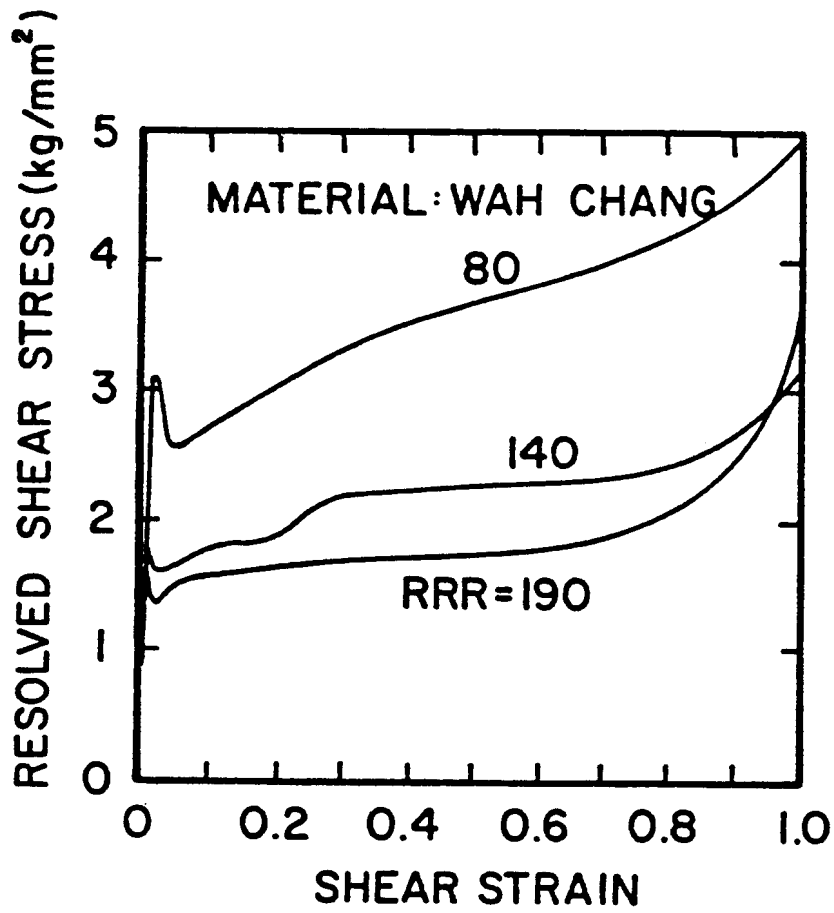


Fig. 7. Electron beam cold hearth furnace.

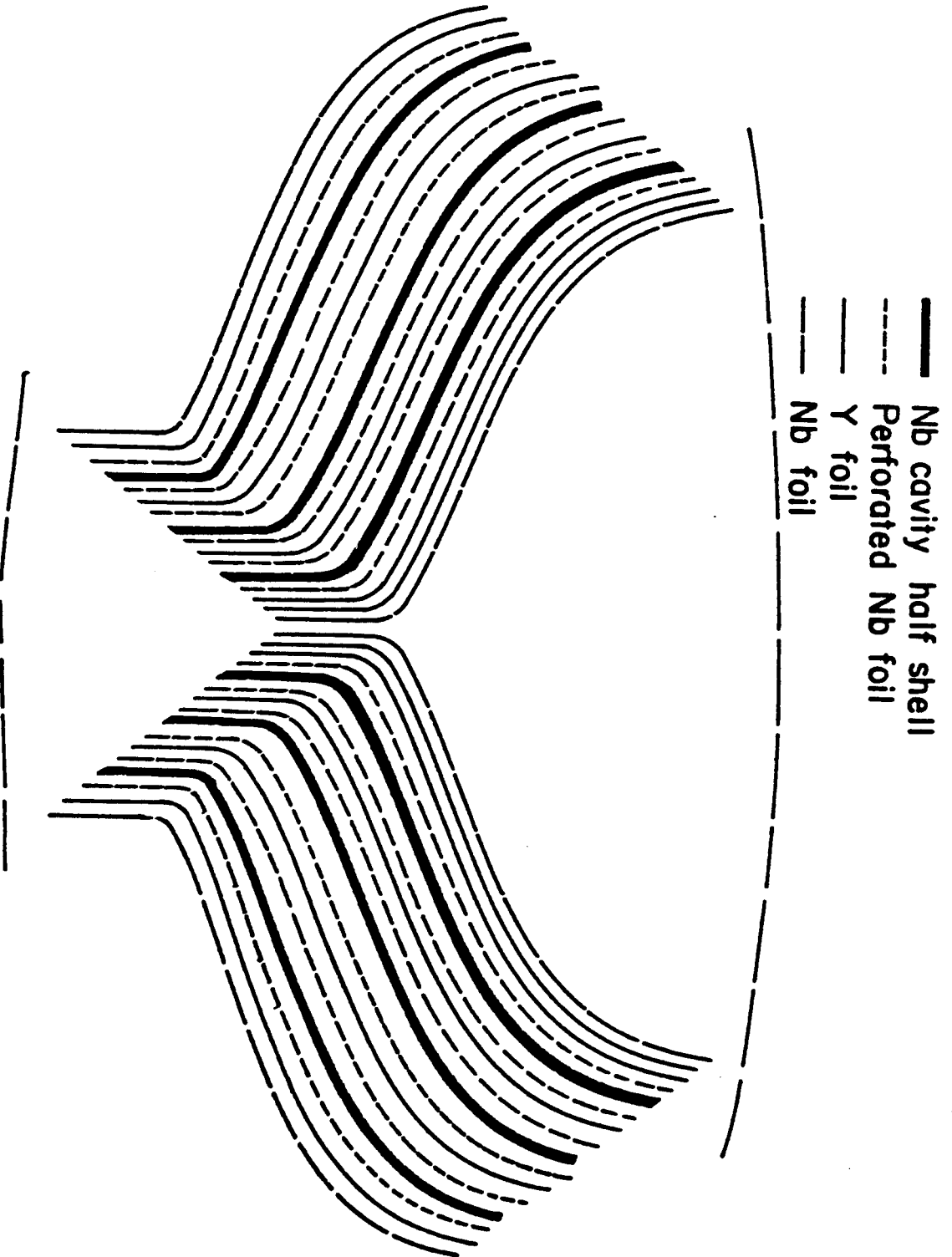
1020784-010



1620784-017

Fig. 9. Effect of Improved purity on the stress-strain curves of Nb.

Fig. 10. Stacking arrangement for purifying Nb cavity half shells by the Yttrium treatment.



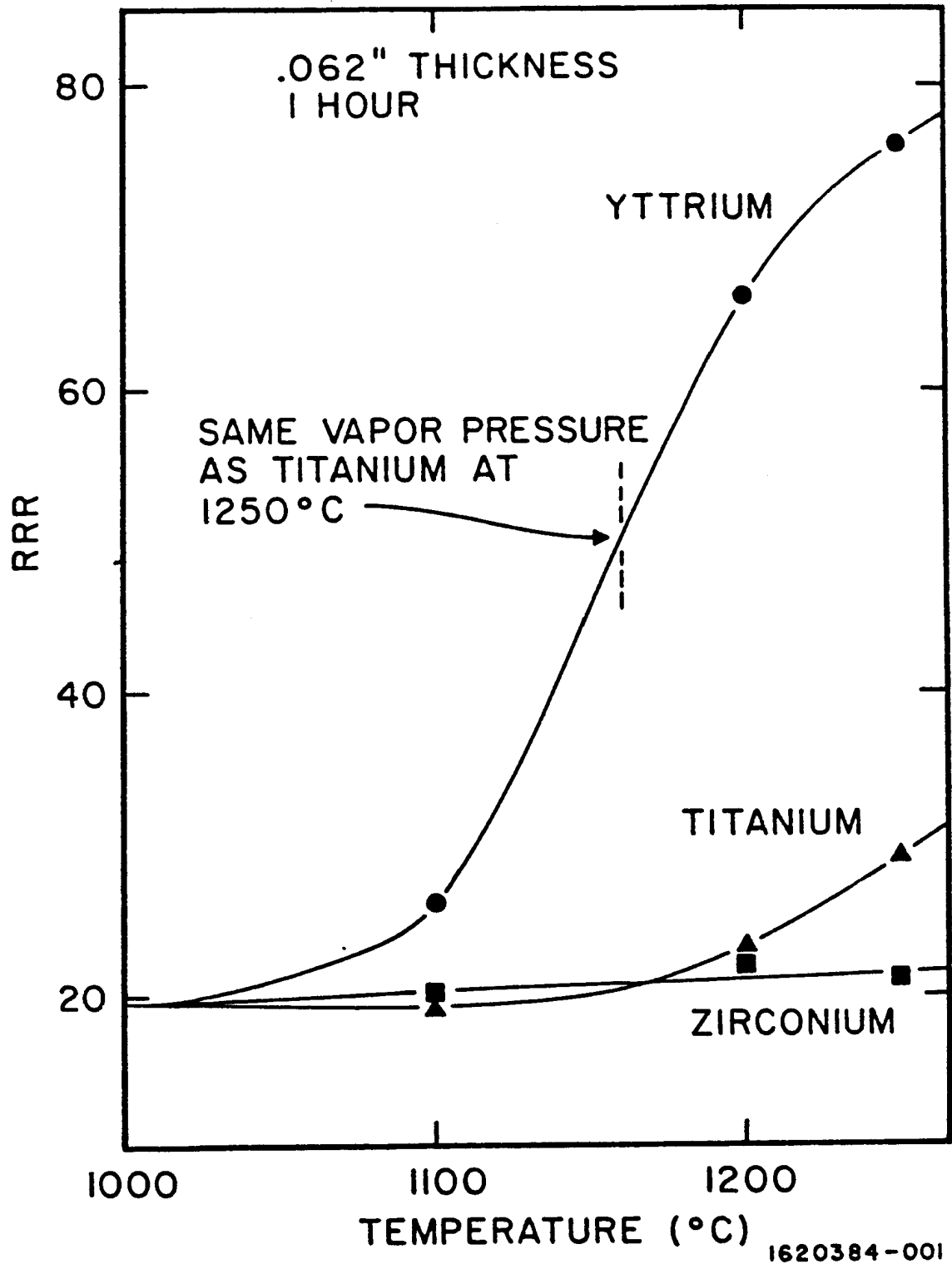


Fig. 11. A comparison between Y, Ti and Zr for the effectiveness of purifying Nb.

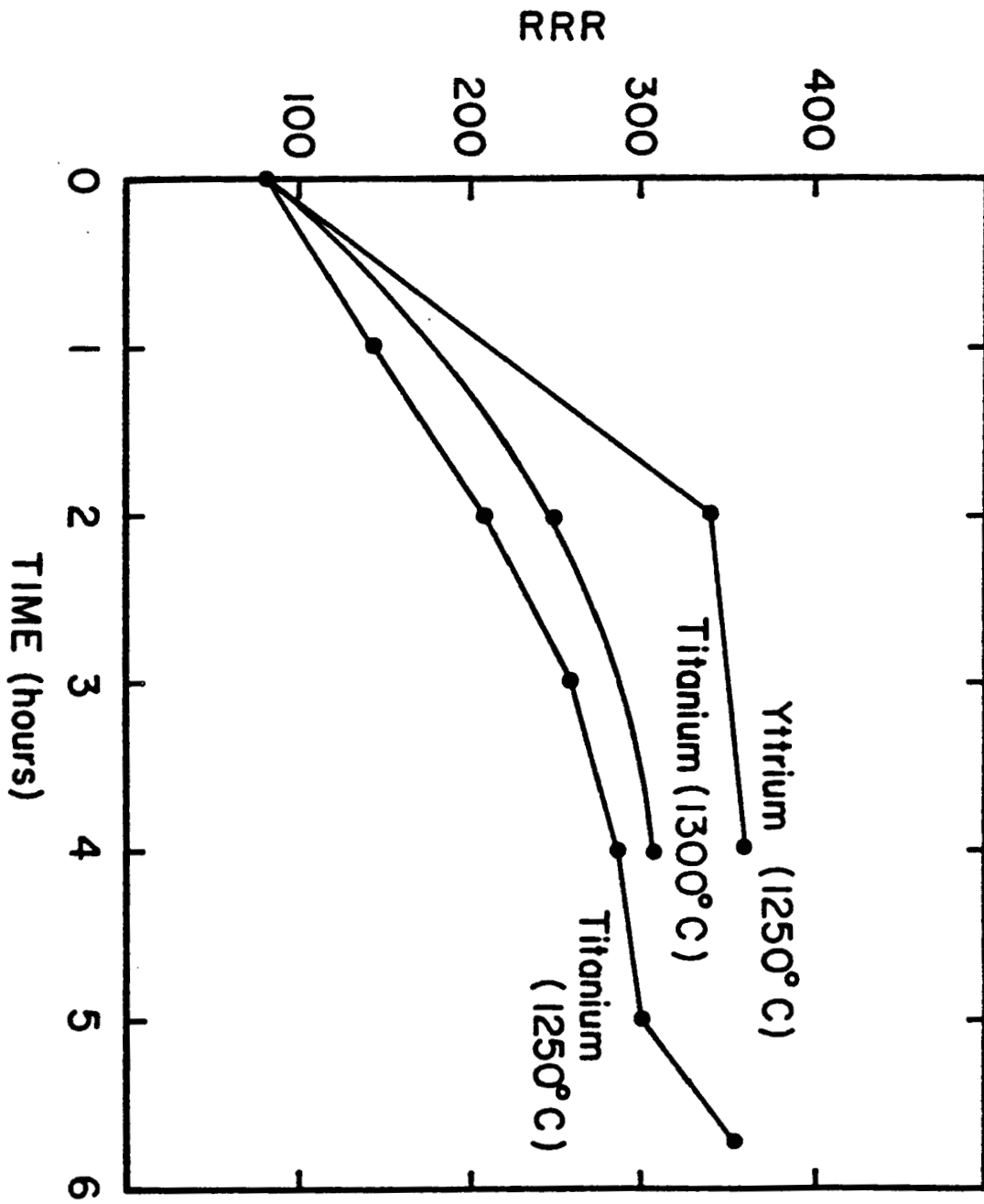
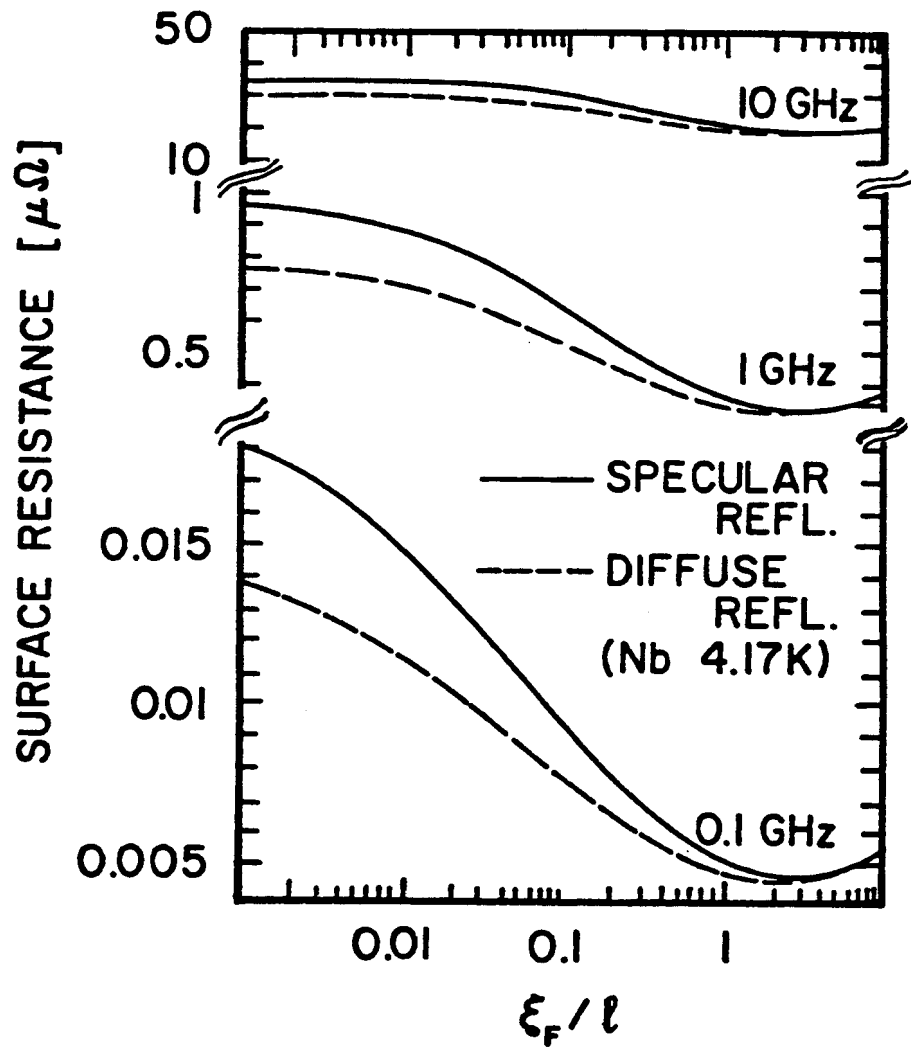


Fig. 12. Purification of Titanium



1620784-016

Fig. 13. Effect of electron mean free path on the BCS surface resistance of Nb.

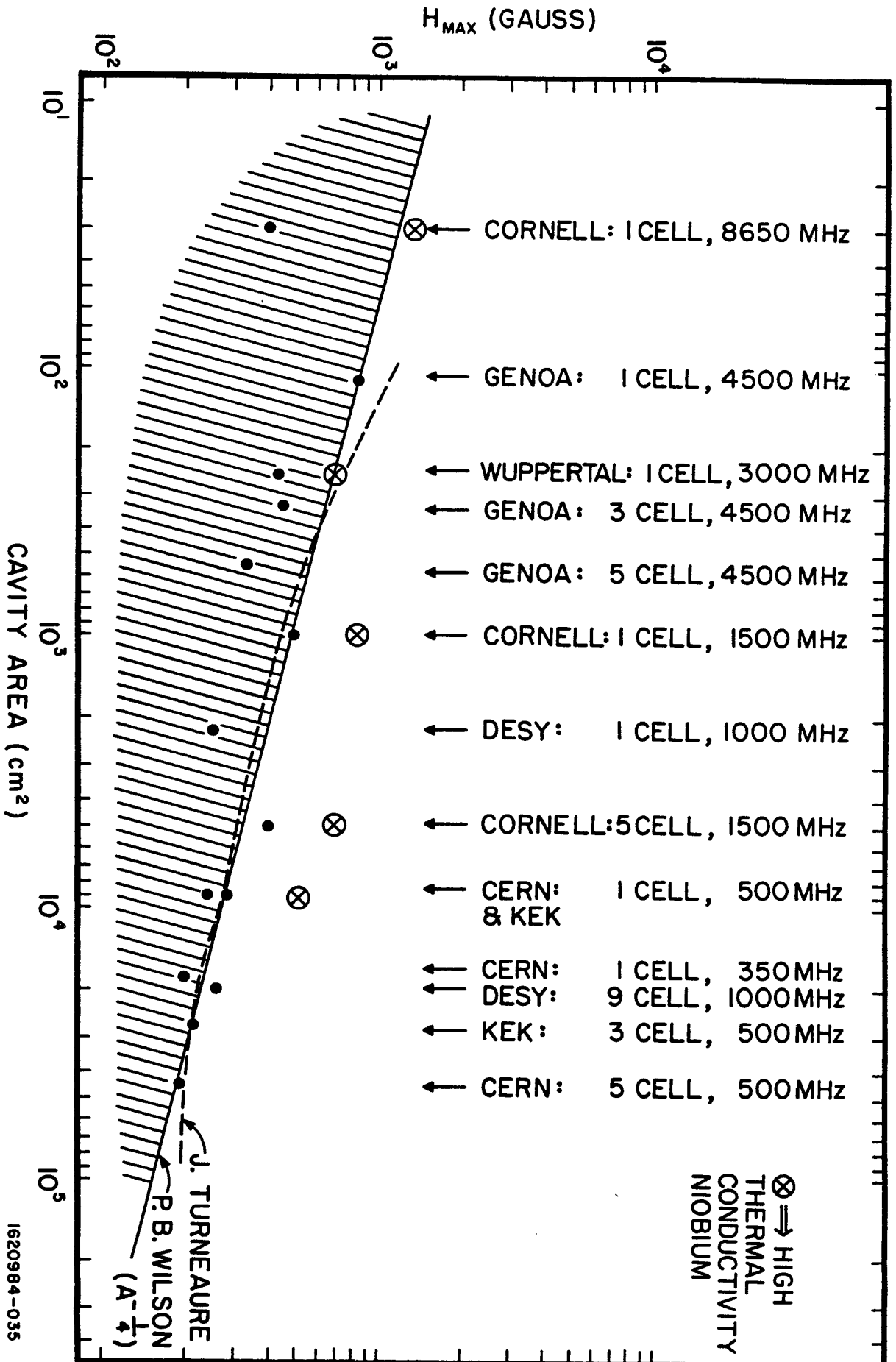


Figure 14. Best results on spherical and elliptical cavities made from low RRR Nb compared with recent best results on high RRR Nb cavities and with statistical breakdown model.

1620984-035